Liquid crystal elastomer self-oscillator with embedded light source

Yong Yu, Fan Yang, Yuntong Dai, and Kai Li [*]

School of Civil Engineering, Anhui Jianzhu University, Hefei, Anhui 230601, China

Light sources that switch periodically over time have a wide range of application value in life and engineering, and generally require additional controller to periodically switch circuits to achieve periodic lighting. In this paper, a self-oscillating spring oscillator based on optically responsive liquid crystal elastomer (LCE) fiber is constructed, which consists of a embedded light source and a LCE fiber. The spring oscillator can oscillate autonomously to achieve periodic switching of the light source. On the basis of the well-established dynamic LCE model, a nonlinear dynamic model is proposed and its dynamic behavior is studied. Numerical calculations demonstrate that the spring oscillator presents two motion regimes, namely the self-oscillation regime and the static regime. The self-oscillation of spring oscillator is maintained by the energy competition between light energy and damping dissipation. Furthermore, the critical conditions for triggering self-oscillation are also investigated in detail, as well as the key system parameters that affect its frequency and amplitude. Different from the existing abundant self-oscillating systems, this self-oscillating structure with simple structure and convenient fabrication does not require complex controller to obtain periodic lighting, and it is expected to provide more diversified design ideas for soft robots and sensors.

I. INTRODUCTION

Self-sustained oscillation refers to the continuous and periodic self-oscillation that occur on its own in the absence of external excitations [1–5]. Self-oscillation has properties and characteristics that other motions do not possess. During the self-oscillation, the system can harvest energy directly from a constant environment to maintain its periodic movement [6–9]. Self-oscillation generally has good robustness [10–12]. The period and amplitude of self-oscillation generally depend on the inherent parameters of the system, and are independent of the initial conditions. This self-oscillation phenomenon has a wide range of promising applications in robotics [13–15], biology [12,16], energy absorption [17,18], and machinery [19,20].

In recent years, an increasing number of self-oscillating systems have been made from different stimuli-responsive materials, including thermally responsive polymer materials [21], ion gels [22], hydrogels [23,24], dielectric elastomers [25], etc. Furthermore, on the basis of diverse active materials, there are many self-sustained motion modes. For instances, rolling [21], swinging [26,27], rotating [28,29], contracting [30,31], buckling [32–34], jumping [35,36], curving [37], and even synchronized motion of several coupled self-oscillators [38] have been established.

Among the many active materials, liquid crystal elastomers (LCEs) are advanced bidirectional memory deformable material synthesized from anisotropic rodlike liquid crystal molecules and stretchable long-chain polymers [19,39–41]. When this material is stimulated by light [19], electric field

[42], magnetic field [43], temperature [44], etc., the liquid crystal monomer molecules rotate and deform [45,46], which, from a macro perspective, is the LCE material undergoing rotational deformation. Under a variety of different stimuli, light excitation has the advantages of easy control, high precision, environmental friendliness, and sustainability [47,48]. With these advantages, optically responsive LCE materials have been widely studied [48–55].

At present, although many self-oscillating systems have been established, the multifunctional demand for different applications is increasing, and with the growing number of studies for LCE-based optically fueled self-oscillation systems [56–59], we also need to build more systems to cope with complex and potential applications in the future. Especially, light sources that switch periodically over time have a wide range of application value in life and engineering, and generally require additional controller to periodically switch circuits to achieve periodic lighting. In this paper, we creatively build a spring oscillator composed of LCE fibers to achieve periodic lighting, based on the contraction-expansion self-oscillation of LCE under shading. This system has the advantages of spontaneous periodic lighting, simple structure, and convenient operation, and is expected to broaden the design ideas in soft robotics, energy harvesters, micromachines, and other fields [60,61].

The paper is structured as follows. First, the corresponding theoretical models and calculation formulas are given in Sec. II. Then, the time history curves and the corresponding phase diagrams for the two motion modes are given in Sec. III. The solution method is also given. Then, in Sec. IV, the influences of several system parameters on the amplitude and frequency of self-oscillation are extensively studied, and the triggering conditions for self-oscillation under different
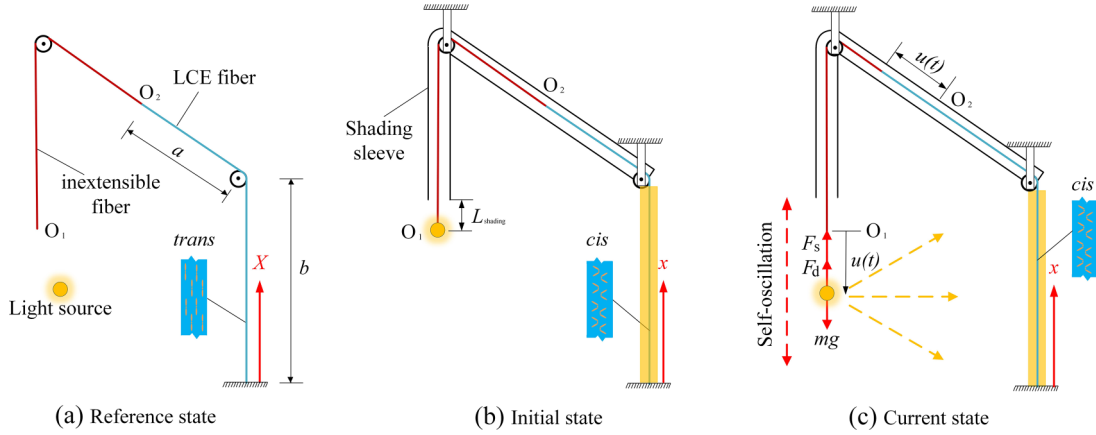
_____

[*]kli@ahjzu.edu.cn

FIG. 1. Schematic diagram of spring oscillator containing optically responsive LCE fiber, inextensible fiber, shading sleeve, and light source: (a) reference state, (b) initial state, and (c) current state. In self-oscillating state, coupling between light-driven contraction of LCE fiber and its motion can trigger self-oscillation of light source.

system parameters are described. Finally, the conclusions are drawn in Sec. V.

II. THEORETICAL MODEL AND FORMULATION

This section proposes a theoretical model of a self-oscillating spring oscillator, including an established particle dynamics model and a dynamic LCE model [46]. The main contents include the dynamics of light source, the tension of the LCE fiber, the evolution of the volume fraction of *cis-isomer* in the LCE fiber, the nondimensionalization, and the solution methods of the differential governing equations with variable coefficients.

A. Dynamics of a self-oscillating light source

Figure 1 depicts the self-oscillating spring oscillator, which consists of an optically responsive LCE fiber, an inextensible fiber, a shading sleeve, and a light source. As shown in Fig. 1(a), the original length of the LCE fiber in the reference state is L_0. The mass of the LCE fiber is assumed to be much smaller than the mass of the light source m, and thus it is neglected for simplicity. In the reference state, the photosensitive molecules such as azobenzene molecules in the LCE fiber are oriented along the fiber axis [19,62–64]. Being a well-known phenomenon, the LCE fiber will contract in illumination (wavelength less than 400 nm) due to the transformation of azobenzene liquid crystal molecules from a straight *trans* state to a bent *cis* state, while the light-driven contraction will recover in darkness due to the transformation of azobenzene liquid crystal molecules from a bent *cis* state to a straight *trans* state [19,62–64].

Initially, the light source is located at position O_1 with an initial velocity of zero. The distance between O_1 and the end of the shading sleeve is denoted by the shadow length $L_{shading}$, as shown in Fig. 1(b). Assuming that the diameter of the fiber is much smaller than the characteristic penetration depth of light, the LCE fiber can only contract longitudinally under illumination due to the transformation of azobenzene liquid crystal molecules from a straight *trans* state to a bent *cis* state. In contrast, in nonilluminated areas, the light-driven

contraction of fiber is recovered due to the transformation of azobenzene liquid crystal molecules from a bent *cis* state to a straight *trans* state. For simplicity, we assume that the LCE fiber length is much smaller than the distance between the light source and the fiber, and thus all parts of nonshielded LCE fibers are exposed to the same light intensity I_0. Affected by gravity, the light source initially moves downwards from static state, the LCE fiber is illuminated, causing the LCE fiber to partially contract, increasing the tension of the fiber, and slowing down and rebounding the mass. Then, the light source moves upwards and enters the sleeve area. Subsequently, the LCE fibers return to the nonilluminated state and thus the tension of the fiber decreases. Afterwards, the light source moves downwards and illuminates the LCE fiber again. Finally, the light source oscillates continuously and periodically.

The mass is subjected to the tension F_s from LCE fiber, and damping force F_d from the air and gravity. Considering the velocity of light source is small, it is assumed that the air-damping force F_d is proportional to the velocity of the light source, which is always in the opposite direction to the velocity. According to Newtonian mechanics, the following governing equation holds at any moment during the self-oscillation of the light source:

$$m\ddot{u}(t) = mg - F_s(t) - c\dot{u}(t), \quad (1)$$

where $u(t)$ is the displacement of the light source, g is the gravitational acceleration, c is the damping coefficient, $\dot{u}$ and $\ddot{u}$ indicate the velocity $\frac{du(t)}{dt}$ and acceleration $\frac{d^2u(t)}{dt^2}$ of the light source, respectively.

For the sake of simplicity, the damping force and the viscosity of the fiber are ignored in this work. For small deformation of the LCE fiber, it is assumed that the tension is proportional to the elastic strain ε_e,

$$F_s(t) = EA\varepsilon_e, \quad (2)$$

where E is the elastic modulus of LCE fiber, and A is the cross-sectional area of LCE fiber. In Eq. (2), the elastic modulus is assumed to be independent of whether it is illuminated or not, and the cross-sectional area A is assumed to remain constant when subjected to tension for small deformation of

LCE fiber. It is worth noting that the elastic strain ε_e in LCE fiber is uniform due to that the tension of the fiber $F_s(t)$ is uniform, while both the total strain ε_{tot} and the light-driven contraction ε_L are nonuniform. To analyze the nonuniform deformation of LCE fiber, we introduce the Lagrange arc coordinate system X in the reference state and the Eulerian arc coordinate system x in the current state. During the self-oscillation, the instantaneous position of a material point in the LCE fiber can be described as $x = x(X, t)$. For simplicity, the elastic strain of LCE fiber ε_e under small deformation can be assumed as a linear combination of the total strain ε_{tot} and the light-driven contraction ε_L, $\varepsilon_e = \varepsilon_{tot} - \varepsilon_L$; thus, the tension can be rewritten as

$$F_s(t) = EA(\varepsilon_{tot} - \varepsilon_L), \tag{3}$$

where ε_L is assumed to be a linear function of the volume fraction of *cis-isomers* $\varphi(X, t)$. Considering that the volume fraction of azobenzene is assumed to be far less than 1, the light-driven contraction strain $\varepsilon_L(X, t)$ is assumed to be proportional to the small *cis-isomer* volume fraction $\phi(t)$,

$$\varepsilon_L(X, t) = -C_0\varphi(X, t), \tag{4}$$

where C_0 is the contraction coefficient. For simplicity, the total strain is defined as $\varepsilon_{tot}(X, t) = \lambda(X, t) - 1$, where the deformation gradient $\lambda(X, t)$ is defined as $\lambda(X, t) = \frac{dx(X,t)}{dX}$. Thus, Eq. (3) can be rewritten as

$$F_s(t) = EA[\lambda(X, t) - 1 + C_0\varphi(X, t)]. \tag{5}$$

To obtain the instantaneous position x of the LCE fiber at any time, by integrating both sides of Eq. (5) from 0 to L_0, we can obtain

$$F_s(t) = \frac{EA}{L_0}\left[u(t) + \int_0^{L_0} C_0\varphi(X, t)dX\right]. \tag{6}$$

From Eq. (5), $\lambda(X, t)$ can be represented by $F_s(t)$

$$\lambda(X, t) = \frac{F_s(t)}{EA} + 1 - C_0\varphi(X, t). \tag{7}$$

Combining Eqs. (3), (6), and (7), we can get

$dx(X, t)$
$$= \left[\frac{1}{L_0}\left(u(t) + \int_0^{L_0} C_0\varphi(X, t)dX\right) + 1 - C_0\varphi(X, t)\right]dX. \tag{8}$$

Integrating both sides of the above formula from 0 to X, we can get

$x(X, t)$
$$= \frac{X}{L_0}\left[u(t) + \int_0^{L_0} C_0\varphi(X, t)dX\right] + X - \int_0^X C_0\varphi(X, t)dX. \tag{9}$$

B. Dynamic LCE model of the fiber

We can make use of the dynamic LCE model proposed by Finkelmann *et al.* [64] to calculate the volume fraction of *cis-isomers* in the LCE fiber. In Eq. (4), $\varphi(X, t)$ generally relies on thermal excitation from *trans* to *cis*, thermally driven relaxation from *cis* to *trans*, and light-driven isomerization.

The thermal excitation from *trans* to *cis* is usually negligible relative to the light-driven excitation. In this paper, we use the following control equation to describe the evolution of the volume fraction of *cis-isomers*:

$$\frac{\partial\varphi(X, t)}{\partial t} = \eta_0 I_0(X, t)[1 - \varphi(X, t)] - T_0^{-1}\varphi(X, t), \tag{10}$$

where η_0 is the light absorption constant and T_0 is the thermal relaxation time from *cis* to *trans*.

C. Nondimensionalization

For convenience, we define the following dimensionless parameters:

$$\tilde{t} = \frac{t}{T_0}, \quad \tilde{F}_s = \frac{F_S T_0^2}{mL_0}, \quad \tilde{X} = \frac{X}{L_0}, \quad \tilde{u} = \frac{u}{L_0},$$

$$\tilde{b} = \frac{b}{L_0}, \quad \tilde{x} = \frac{x}{L_0}, \quad \tilde{L}_{shading} = \frac{L_{shading}}{L_0},$$

$$\tilde{c} = \frac{cT_0}{m}, \quad \tilde{g} = \frac{gT_0^2}{L_0}, \quad \tilde{E} = \frac{EAT_0^2}{mL_0},$$

and $\tilde{I}(x) = T_0\eta_0 I(x)$. Equation (1) can be expressed as

$$\ddot{\tilde{u}} = \tilde{g} - \tilde{E}\left[\tilde{u}(\tilde{t}) + \int_0^1 C_0\varphi(\tilde{X}, \tilde{t})\right] - \tilde{c}\dot{\tilde{u}}_0. \tag{11}$$

Equation (9) can be expressed as

$$\tilde{x}(\tilde{X}, \tilde{t}) = \tilde{X}\left[\tilde{u}(\tilde{t}) + \int_0^1 C_0\varphi(\tilde{X}, \tilde{t})d\tilde{X}\right]$$
$$- \int_0^{\tilde{X}} C_0\varphi(\tilde{X}, \tilde{t})d\tilde{X} + \tilde{X}. \tag{12}$$

Equation (10) can be expressed as

$$\frac{\partial\varphi(\tilde{X}, \tilde{t})}{\partial\tilde{t}} = \tilde{I}(\tilde{X}, \tilde{t})[1 - \varphi(\tilde{X}, \tilde{t})] - \varphi(\tilde{X}, \tilde{t}). \tag{13}$$

Equation (6) can be expressed as

$$\tilde{F}_s(\tilde{t}) = \tilde{E}\left[\tilde{u}(\tilde{t}) + \int_0^1 C_0\varphi(\tilde{X}, \tilde{t})\right]. \tag{14}$$

Equation (11) is the dynamic equation of the system, Eq. (12) controls the current position of each material point, and Eq. (13) represents the volume fraction of *cis-isomers* in the LCE fiber. The calculated value of $\tilde{x}$ from Eq. (12) can be used to determine whether the material point of the LCE fiber is in illumination or darkness. Equations (11) and (13) govern the self-oscillation of this system. To solve these complex differential equations with variable coefficients, the Runge-Kutta method is used and numerical calculation is carried out in MATLAB software. For the volume fraction ϕ_i according to the illumination time of the LCE material at t_i time, the current tension of the LCE fiber $\tilde{F}_{si}$ can be determined by Eq. (14). Given the initial conditions, iterating through Eq. (12) to determine the current position $\tilde{x}_i(\tilde{X}, \tilde{t}_i)$ and estimate the light intensity $\tilde{I}(\tilde{X}, \tilde{t}_i)$, then from Eq. (13), the volume fraction ϕ_i can be calculated, and $\tilde{u}, \tilde{\dot{u}}_0$ can be calculated. Thus, for given parameters $C_0, \tilde{I}_0, \tilde{E}, \tilde{c}, \tilde{b}, \tilde{L}_{shading}$, and $\tilde{g}$, iterative calculations can be performed to obtain the dynamics of the self-oscillation of this system.

TABLE I. Material properties and geometric parameters.

Parameter	Definition	Value	Unit
C_0	Contraction coefficient	0–0.12	
c	Damping coefficient	0–0.01	kg/s
b	Illumination length	0–0.7	m
E	Elastic modulus of LCE fiber	0–5	MPa
A	Cross-sectional area of LCE fiber	0–2	mm^2
T_0	Thermal relaxation time	0–0.2	s
L_0	Original length of LCE fiber	1	m
g	Gravitational acceleration	0–20	m/s^2
m	Mass of light source	0–0.1	kg
η_0	Light-absorption constant	0.0003	m^2/(s W)
I_0	Light intensity	0~20	kW/m^2

III. TWO MOTION REGIMES AND MECHANISM OF SELF-OSCILLATION

In this section, by solving the governing Eqs. (11) and (13), we first present two typical motion regimes, which are distinguished as the static regime and the self-oscillation regime. Next, the corresponding mechanism of the self-oscillation of light source is elucidated in detail.

A. Two motion regimes

To investigate the properties of self-oscillating light source suspended by LCE fiber, it is necessary to determine the typical values of dimensionless parameters in the model. Typical material properties and geometric parameters are presented in Table I [8,63,64]. The corresponding dimensionless parameters are also listed in Table II. In the following, these parameter values are used to study the self-oscillation of light source.

Figure 2 depicts the two typical motion regimes of the light source suspended by a LCE fiber, i.e., the self-oscillation regime [Fig. 2(a)] and the static regime [Fig. 2(c)]. In the computation, we set $\tilde{E} = 4$, $\tilde{I} = 0.1$, $\tilde{g} = 0.1$, $C_0 = 0.1$, $\tilde{b} = 0.5$, and $\tilde{L}_{\text{shading}} = 0$. By numerically solving the governing equations (12) and (13), we can obtain the time history curve and the limit cycle of the suspended light source. For $\tilde{c} = 0.05$, the light source eventually developed into self-oscillation under the action of gravity and tension of the LCE fiber, as shown in Fig. 2(a) [65], and the phase trajectory evolves in the phase plane to form a limit cycle, as shown in Fig. 2(b). For $\tilde{c} = 0.15$, the light source vibrates up and down under the action of gravity and tension of the LCE fiber, and then quickly develops into a static regime due to system damping, as shown in Fig. 2(c). Figure 2(d) shows the phase trajectory corresponding to the static regime, which is ultimately maintained at a static point in Fig. 2(d).

TABLE II. Dimensionless parameters.

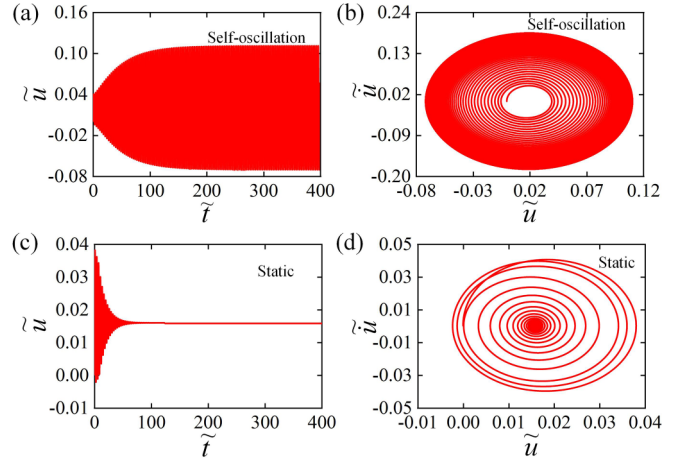| Parameter	$\tilde{I}$	$\tilde{c}$	$\tilde{g}$	C_0	$\tilde{E}$	$\tilde{b}$	$\tilde{L}_{\text{shading}}$
Value	0–1	0–0.05	0–0.5	0–0.12	0–5	0–0.7	0–0.1

FIG. 2. Two motion regimes of light source suspended by LCE fiber: (a), (b) Self-oscillation regime ($\tilde{c} = 0.05$); (c), (d) static regime ($\tilde{c} = 0.15$). The other dimensionless parameters are $\tilde{E} = 4$, $\tilde{I} = 0.1$, $\tilde{g} = 0.1$, $C_0 = 0.1$, $\tilde{b} = 0.5$, $\tilde{L}_{\text{shading}} = 0$. Video 1 present two motion regimes. See Supplemental Material for videos associated some of the figures [65].

B. Mechanism of self-oscillation

To elucidate the mechanism of self-oscillation of the suspended light source, Figs. 3(a)–3(c) present the time history curves of several key physical quantities for $\tilde{E} = 4$, $\tilde{I} = 0.1$, $\tilde{g} = 0.1$, $C_0 = 0.1$, $\tilde{b} = 0.5$, $\tilde{L}_{\text{shading}} = 0$, and $\tilde{c} = 0.05$. The volume fraction of *cis-isomers*, displacement, and tension of the fiber of the self-oscillating suspended light source all vary periodically with time. Figure 3(d) describes the variation of the tension of the fiber with displacement. The yellow-shaded areas in Fig. 3(a) indicate that the LCE fiber is exposed to illumination. In Fig. 3(a), when the material point moves into the
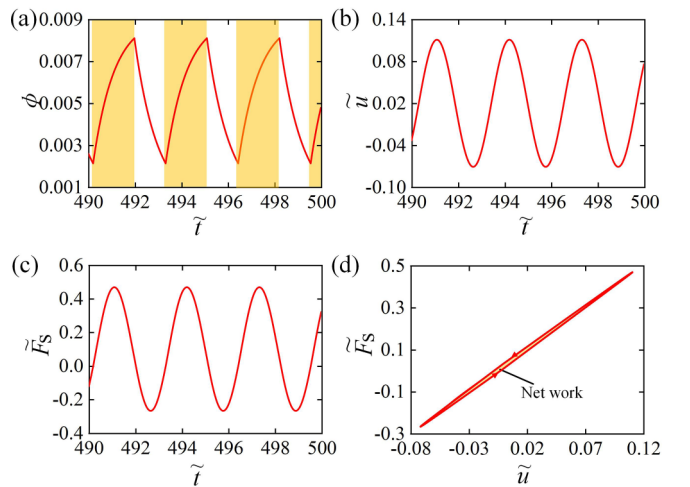

FIG. 3. Mechanism of self-oscillation of suspended light source. (a) Variation of volume fraction of *cis-isomers* in with time; (b) dependence between displacement of self-oscillating suspended light source and time; (c) dependence between tension and time; and (d) dependence between tension and displacement. Parameters are set as $\tilde{E} = 4$, $\tilde{I} = 0.1$, $\tilde{g} = 0.1$, $C_0 = 0.1$, $\tilde{b} = 0.5$, $\tilde{L}_{\text{shading}} = 0$, and $\tilde{c} = 0.05$.
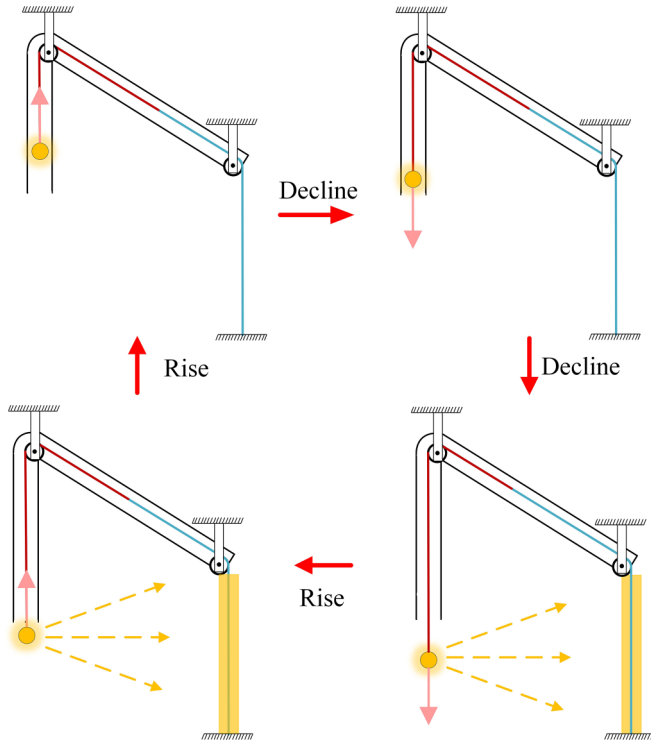
FIG. 4. Snapshots of self-oscillating suspended light source in one cycle shown in Figs. 2(a) and 2(b). Suspended light source exhibits continuous periodic self-oscillating due to periodic change in light-driven contraction of LCE fiber.

illumination, ϕ gradually increases with time and approaches a limit value, while ϕ gradually decreases in the darkness. Both $\tilde{u}$ and $\tilde{F}$ exhibit periodic behavior due to the periodic variation in the volume fraction of *cis-isomers* ϕ, as shown in Figs. 3(b) and 3(c). In Fig. 3(d), the closed region enclosed by the tension and displacement represents the energy loss of the light source that compensates for the damping dissipation to maintain the periodic self-oscillation of the system, which can be further understood from Fig. 4. Given this self-oscillation mechanism, it is possible to keep the system maintaining stable self-oscillation when we set parameters that allow the net work invested in the system to balance the energy dissipated by the damping.

IV. EFFECTS OF SYSTEM PARAMETERS ON THE SELF-OSCILLATION

In the above self-oscillating mechanical model, there are seven dimensionless system parameters, including C_0, $\tilde{I}$, $\tilde{c}$, $\tilde{E}$, $\tilde{b}$, $\tilde{L}_{\text{shading}}$, and $\tilde{g}$. This section examines in detail the influences of these system parameters on the triggering conditions, frequency, and amplitude of the self-oscillation. The dimensionless self-oscillation frequency and amplitude are denoted by f and A, respectively.

A. Effect of the elastic modulus

Figure 5 and Video 2 [65] describe the effect of elastic modulus on the self-oscillating light source. Figure 5(a) plots the limit cycles corresponding to different elastic moduli. The
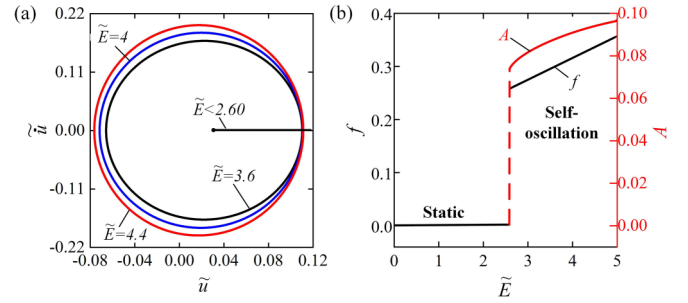

FIG. 5. Effect of elastic modulus on self-oscillating light source, for $C_0 = 0.1$, $\tilde{I} = 0.1$, $\tilde{c} = 0.05$, $\tilde{b} = 0.5$, $\tilde{L}_{\text{shading}} = 0$, and $\tilde{g} = 0.1$. (a) Limit cycles. (b) Frequency and amplitude. Critical elastic modulus for triggering self-oscillation is about $\tilde{E} = 2.6$. With increase of elastic modulus, amplitude and frequency show upward trend.

critical elastic modulus for triggering the self-oscillation of the light source is approximately $\tilde{E} = 2.6$. In other words, for $\tilde{E} < 2.6$, the system is static, while for $\tilde{E} > 2.6$, the system eventually evolves into a self-oscillating state. Figure 5(b) provides the frequency and amplitude of self-oscillation as functions of the elastic modulus $\tilde{E}$. As $\tilde{E}$ increases, the amplitude tends to rise and the frequency also shows an upward trend. With the increase of $\tilde{E}$, LCE fiber with higher elastic modulus is more suitable for converting light energy into mechanical energy. Increasing the elastic modulus of LCE material can simultaneously increase the frequency and amplitude of the system to adapt to different engineering applications.

B. Effect of the light intensity

Figure 6 and Video 3 [65] describe the effect of light intensity on the self-oscillating light source. Figure 6(a) plots the limit cycles corresponding to different light intensities. The critical value of light intensity to trigger the self-oscillation of the light source is approximately $\tilde{I} = 0.054$. That is, for $\tilde{I} < 0.054$, the system exhibits static state, while for $\tilde{I} > 0.054$, the system exhibits self-oscillating state. Figure 6(b) provides the dependences between frequency and amplitude of self-oscillation and light intensity $\tilde{I}$. With the increasing $\tilde{I}$,
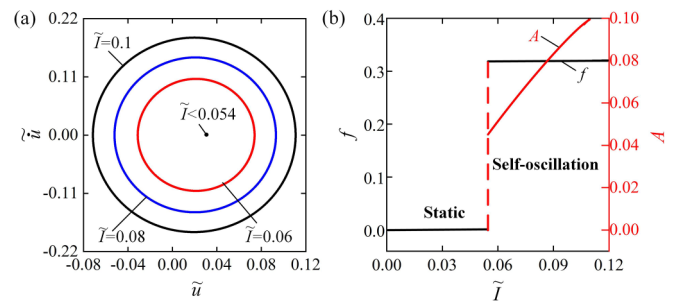

FIG. 6. Effect of light intensity on self-oscillating light source, for $C_0 = 0.1$, $\tilde{E} = 4$, $\tilde{c} = 0.05$, $\tilde{b} = 0.5$, $\tilde{L}_{\text{shading}} = 0$, and $\tilde{g} = 0.1$. (a) Limit cycles. (b) Frequency and amplitude. Critical light intensity that triggers self-oscillation is approximately $\tilde{I} = 0.054$. With increase of light intensity, amplitude tends to increase, while frequency remains almost constant.
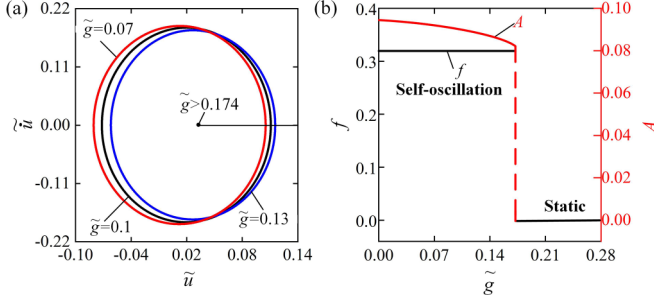
FIG. 7. Effect of gravitational acceleration on self-oscillating light source, for $\tilde{E} = 4$, $\tilde{I} = 0.1$, $\tilde{c} = 0.05$, $\tilde{b} = 0.5$, $\tilde{L}_{\text{shading}} = 0$, and $C_0 = 0.1$. (a) Limit cycles. (b) Frequency and amplitude. There exists critical gravitational acceleration, approximately $\tilde{g} = 0.174$, to trigger self-oscillation. As gravitational acceleration increases, amplitude shows decreasing trend, while frequency does not change.
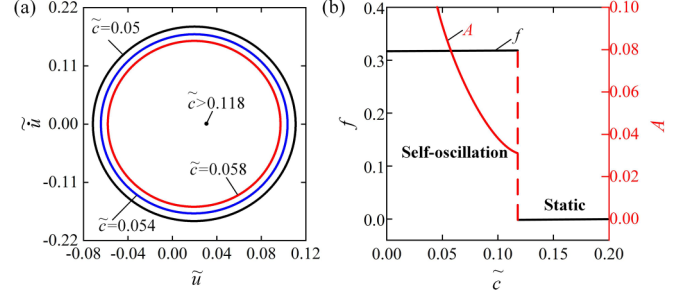

FIG. 8. Effect of damping coefficient on self-oscillating light source, for $\tilde{E} = 4$, $\tilde{I} = 0.1$, $\tilde{b} = 0.5$, $\tilde{L}_{\text{shading}} = 0$, $C_0 = 0.1$, and $\tilde{g} = 0.1$. (a) Limit cycles. (b) Frequency and amplitude. Damping coefficient for triggering self-oscillation has critical value of approximately $\tilde{c} = 0.118$. With increase of damping coefficient, amplitude presents decreasing trend, while frequency does not change.

the amplitude tends to increase, while the frequency remains almost constant. The energy absorbed by the system increases as $\tilde{I}$ increases, so the amplitude increases, while the frequency is almost unchanged. This is the result of the conversion of light energy into mechanical energy. We can adapt to different complex scenes by changing the light intensity.

C. Effect of the gravitational acceleration

Figure 7 and Video 4 [65] describe the effect of gravitational acceleration on the self-oscillating light source. The limit cycles corresponding to different gravitational accelerations are plotted in Fig. 7(a). There exists a critical gravitational acceleration, approximately $\tilde{g} = 0.174$, to trigger the self-oscillation of the light source. This means that for $\tilde{g} > 0.174$, the system is static, while for $\tilde{g} < 0.174$, the system eventually evolves into a self-oscillating state. Figure 7(b) presents the variations of frequency and amplitude of self-oscillation with gravitational acceleration $\tilde{g}$. When $\tilde{g}$ is increased, the amplitude shows a decreasing trend, while the frequency does not change. The larger the gravitational acceleration, the lower the equilibrium position; the fewer fibers there will be in the illumination area, the less work will be done by the fiber, and consequently the input energy is reduced during self-oscillation.

D. Effect of the damping coefficient

Figure 8 and Video 5 [65] describe the effect of damping coefficient on the self-oscillating light source. Figure 8(a) plots the limit cycles corresponding to different damping coefficients. The damping coefficient for triggering the self-oscillation of the light source has a critical value of approximately $\tilde{c} = 0.118$. To put it another way, for $\tilde{c} > 0.118$, the system is in static regime, while for $\tilde{c} < 0.118$, the system is in self-oscillation regime. Figure 8(b) provides the frequency and amplitude of self-oscillation as functions of the damping coefficient $\tilde{c}$. With the increase of $\tilde{c}$, the amplitude presents a decreasing trend, while the frequency does not change. When $\tilde{c} > 0.118$, the input energy is not sufficient to compensate for the damping dissipation; the system appears static. An appropriate reduction in the damping coefficient

can improve the efficiency of converting light energy into mechanical energy.

E. Effect of the contraction coefficient

Figure 9 and Video 6 [65] describe the effect of contraction coefficient on the self-oscillating light source. The limit cycles corresponding to different contraction coefficients are given in Fig. 9(a). The critical value of contraction coefficient to trigger the self-oscillation of the light source is approximately $C_0 = 0.057$. In other words, for $C_0 < 0.057$, the system is static, while for $C_0 > 0.057$, the system eventually evolves into self-oscillation. Figure 9(b) demonstrates how the frequency and amplitude of self-oscillation vary with the contraction coefficient C_0. As C_0 increases, there is a clear upward trend in amplitude, while the frequency does not change. Equation (4) provides a basis for the fact that with the increase of C_0, the light-driven contraction increases; therefore, the amplitude of self-oscillation increases. Increasing the contraction coefficient of LCE materials can improve the conversion efficiency of light energy to mechanical energy.
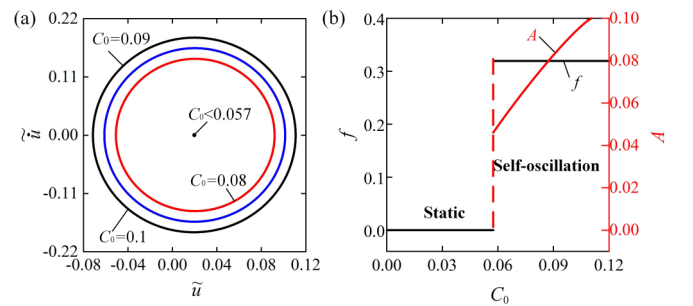

FIG. 9. Effect of contraction coefficient on self-oscillating light source, for $\tilde{E} = 4$, $\tilde{I} = 0.1$, $\tilde{c} = 0.05$, $\tilde{b} = 0.5$, $\tilde{L}_{\text{shading}} = 0$, and $\tilde{g} = 0.1$. (a) Limit cycles. (b) Frequency and amplitude. Critical value of contraction coefficient to trigger self-oscillation is approximately $C_0 = 0.057$. When contraction coefficient is increased, there is clear upward trend in amplitude, while frequency does not change.
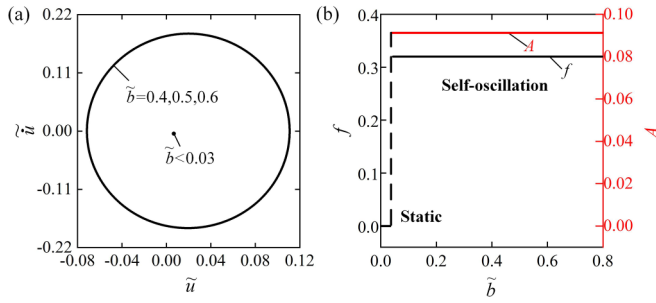
FIG. 10. Effect of illumination length on self-oscillating light source, for $\tilde{E} = 4$, $\tilde{I} = 0.1$, $C_0 = 0.1$, $c = 0.2$, $\tilde{L}_{shading} = 0$, and $\tilde{g} = 0.1$. (a) Limit cycles. (b) Frequency and amplitude. Presence of critical illumination length that triggers self-oscillation is approximately $\tilde{b} = 0.03$. As illumination length increases, both amplitude and frequency remain constant.
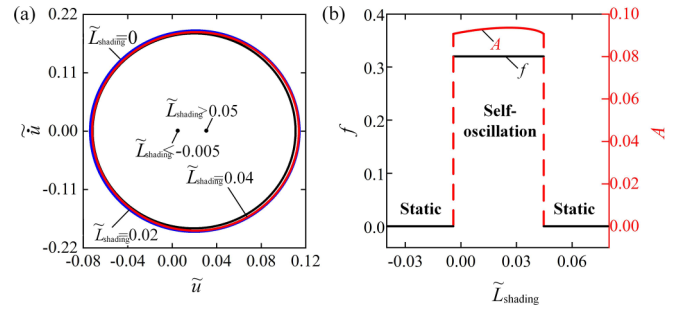

FIG. 11. Effect of shading length on self-oscillating light source, for $\tilde{E} = 4$, $\tilde{I} = 0.1$, $\tilde{c} = 0.05$, $\tilde{b} = 0.5$, $C_0 = 0.1$, and $\tilde{g} = 0.1$. (a) Limit cycles. (b) Frequency and amplitude. There are two critical shading lengths for triggering self-oscillation, which are approximately $\tilde{L}_{shading} = -0.005$ and $\tilde{L}_{shading} = 0.05$. With increase of shading length, amplitude shows trend of rise first and then decrease, while frequency is almost constant.

F. Effect of the illumination length

Figure 10 and Video 7 [65] describe the effect of illumination length on the self-oscillating light source. Figure 10(a) plots the limit cycles corresponding to different illumination lengths. The critical illumination length triggering the self-oscillation of the light source is approximately $\tilde{b} = 0.03$. That is to say, for $\tilde{b} < 0.03$, the system exhibits static state, while for $\tilde{b} > 0.03$, the system eventually evolves into a self-oscillating state. The dependences between frequency and amplitude of self-oscillation and illumination length $\tilde{b}$ are given in Fig. 10(b). With the increase of $\tilde{b}$, both amplitude and frequency remain constant. As the illumination length increases, the illumination length meets the system's demand for light, and the amplitude and frequency of the self-oscillating light source remain unchanged. We can reduce the illumination length so as to improve the utilization rate of LCE materials.

G. Effect of the shading length

Figure 11 and Video 8 [65] describe the effect of shading length on the self-oscillating light source. Figure 11(a) plots the limit cycles corresponding to different shading lengths. The two critical shading lengths that trigger the self-oscillation of the suspended light source are approximately $\tilde{L}_{shading} = -0.005$ and $\tilde{L}_{shading} = 0.05$. This means that for $\tilde{L}_{shading} < -0.005$ and $\tilde{L}_{shading} > 0.05$, the system is static, while for $-0.005 < \tilde{L}_{shading} < 0.05$, the system eventually develops into self-oscillation. Figure 11(b) provides the frequency and amplitude of self-oscillation as functions of shading length $\tilde{L}_{shading}$. As $\tilde{L}_{shading}$ increases, the amplitude shows a trend of rise first and then decrease, while the frequency is almost constant. Therefore, in practice, proper adjustment of the shadow length is one of the effective measures to improve the self-oscillation amplitude.

V. CONCLUSIONS

Light source based on periodic switching has a wide range of applications in life and engineering. This paper creatively proposes a self-oscillating spring oscillator to achieving periodic lighting without additional controller, which consists of a LCE fiber, an inextensible fiber, a shading sleeve, and a light source. Considering the established particle dynamics model and the dynamic LCE model, the governing equation of the self-oscillating spring oscillator is established and the self-oscillation under steady-state illumination are studied. Numerical calculations demonstrate that the amplitude and frequency of the self-oscillation are influenced by multiple system parameters. Increasing the system parameters, including C_0, $\tilde{I}$, and $\tilde{E}$, can improve the amplitude. However, C_0 and $\tilde{I}$ cause the frequency to be constant, and $\tilde{E}$ makes the frequency go upward. With the increases of $\tilde{g}$ and $\tilde{c}$, the amplitude decreases, while $\tilde{g}$ and $\tilde{c}$ cause the frequency to constant. The increase of $\tilde{b}$ makes both amplitude and frequency constant. With the increases of $\tilde{L}_{shading}$, the amplitude increases first and then decreases, and the frequency remains constant. The self-oscillating spring oscillator constructed in the current paper has the advantages of simple structure, easy preparation, and strong operability, which have great application prospects in the fields of soft robotics, micromachines, and sensors.

[1] W. J. Ding, *Self-Excited Vibration* (Tsing-Hua University Press, BeiJing, 2009).

[2] F. Ge, R. Yang, X. Tong, F. Camerel, and Y. Zhao, A multifunctional dye-doped liquid crystal polymer actuator: Light-guided transportation, turning in locomotion, and autonomous motion, Angew. Chem. Int. Ed. **57**, 11758 (2018).

[3] A. Jenkins, Self-oscillation, Phys. Rep. **525**, 167 (2013).

[4] M. Li, H. P. Keller, B. Li, X. Wang, and M. Brunet, Light-driven side-on nematic elastomer actuators, Adv. Mater. **15**, 569 (2003).

[5] X. Wang, C. F. Tan, K. H. Chan, X. Lu, L. Zhu, S. Kim, and G. W. Ho, In-built thermo-mechanical cooperative feedback

mechanism for self-propelled multimodal locomotion and electricity generation, Nat. Commun. **9**, 19881 (2018).

[6] A. Baumann, *Active Motion and Self-Propulsion of Polymers and Fibers Physics* (Université de Strasbourg. NNT, 2018STRAE024, Strasbourg, 2018).

[7] X. Wang and G. W. Ho, Design of untethered soft material micromachine for life-like locomotion, Mater. Today. **53**, 197 (2022).

[8] C. Du, Q. Cheng, K. Li, and Y. Yu, A light-powered liquid crystal elastomer spring oscillator with self-shading coatings, Polymers **14**, 1525 (2022).

[9] K. Li, Z. Chen, and P. Xu, Light-propelled self-sustained swimming of a liquid crystal elastomer torus at low Reynolds number, Int. J. Mech. Sci. **219**, 107128 (2022).

[10] S. Chatterjee, Self-excited oscillation under nonlinear feedback with time-delay, J. Sound. Vib. **330**, 1860 (2011).

[11] L. Hines, K. Petersen, G. Z. Lum, and M. Sitti, Soft actuators for small-scale robotics, Adv. Mater. **29**, 1603483 (2017).

[12] V. Sangwan, A. Taneja, and S. Mukherjee, Design of a robust self-excited biped walking mechanism, Mech. Mach. Theory **39**, 1385 (2004).

[13] W. Hu, G. Z. Lum, and M. Mastrangeli, Small-scale soft-bodied robot with multimodal locomotion, Nature (London) **554**, 81 (2018).

[14] D. Martella, S. Nocentini, and C. Parmeggiani, Self-regulating capabilities in photonic robotics, Adv. Mater. Technol. **4**, 1800571 (2019).

[15] B. Shin, J. Ha, M. Lee, K. Park, G. H. Park, T. H. Choi, K. J. Cho, and H. M. Kim, Hygrobot: A self-locomotive ratcheted actuator powered by environmental humidity, Sci. Robot. **3**, eaar2629 (2018).

[16] K. Kruse and F. Jülicher, Oscillations in cell biology, Curr. Opin, Cell Biol. **17**, 20 (2005).

[17] D. Zhao and Y. Liu, A prototype for light-electric harvester based on light sensitive liquid crystal elastomer cantilever, Energy **198**, 117351 (2020).

[18] S. Serak, R. Vergara N.Tabiryan, T. J. White, R. A. Vaia, and T. J. Bunning, Liquid crystalline polymer cantilever oscillators fueled by light, Soft Matter **6**, 779 (2010).

[19] Y. C. Cheng, H. C. Lu, X. Lee, H. Zeng, and A. Priimagi, Kirigami-based light-induced shape-morphing and locomotion, Adv. Mater. **32**, 1906233 (2020).

[20] P. Rothemund, A. Ainla, L. Belding, D. J. Preston, S. Kurihara, Z. Suo, and G. M. Whitesides, A soft bistable valve for autonomous control of soft actuators, Sci. Robot. **3**, eaar7986 (2018).

[21] Q. Shen, S. Trabia, T. Stalbaum, V. Palmre, K. Kim, and I. K. Oh, A multiple-shape memory polymer-metal composite actuator capable of programmable control, creating complex 3D motion of bending twisting and oscillation, Sci. Rep. **6**, 24462 (2016).

[22] J. Boissonade and P. De. Kepper, Multiple types of spatiotemporal oscillations induced by differential diffusion in the Landolt reaction, Phys. Chem. Chem. Phys. **13**, 4132 (2011).

[23] R. Yoshida, Self-oscillating gels driven by the Belousov–Zhabotinsky reaction as novel smart materials, Adv. Mater. **22**, 3463 (2010).

[24] C. Kim, M. Hua, Y. Du, D. Wu, R. Bai, and X. He, Swaying gel: Chemo-mechanical self-oscillation based on dynamic buckling, Matter **4**, 1029 (2021).

[25] J. Wu, S. Yao, H. Zhang, W. Man, Z. Bai, F. Zhang, Y. Zhang, X. Wang, D. Fang, and Y. Zhang, Liquid crystal elastomer metamaterials with giant biaxial thermal shrinkage for enhancing skin regeneration, Adv. Mater. **33**, 2106175 (2021).

[26] H. Zeng, M. Lahikainen, L. Liu, Z. Ahmed, O. M. Wani, M. Wang, and A. Priimagi, Light-fuelled freestyle self-oscillators, Nat. Commun. **10**, 5057 (2019).

[27] M. Pilz da Cunha, A. R. Peeketi, A. Ramgopal, R. K. Annabattula, and A. P. Schenning, Light-driven continual oscillatory rocking of a polymer film, ChemistryOpen **9**, 1149 (2020).

[28] D. Ge, Y. Dai, and K. Li, Light-powered self-spinning of a button spinner, Int. J. Mech. Sci. **238**, 107824 (2023).

[29] Y. Yu, C. Du, K. Li, and S. Cai, Controllable and versatile self-motivated motion of a fiber on a hot surface, Extreme Mech. Lett. **57**, 101918 (2022).

[30] P. Xu, H. Wu, Y. Dai, and K. Li, Self-sustained chaotic floating of a liquid crystal elastomer balloon under steady illumination, Heliyon **9**, e14447 (2023).

[31] Q. Cheng, W. Cheng, Y. Dai, and K. Li, Self-oscillating floating of a spherical liquid crystal elastomer balloon under steady illumination, Int. J. Mech. Sci. **241**, 107985 (2023).

[32] L. Zhou, Y. Dai, J. Fang, and K. Li, Light-powered self-oscillation in liquid crystal elastomer auxetic metamaterials with large volume change, Int. J. Mech. Sci. **254**, 108423 (2023).

[33] D. Ge and K. Li, Self-oscillating buckling and postbuckling of a liquid crystal elastomer disk under steady illumination, Int. J. Mech. Sci. **221**, 107233 (2022).

[34] D. Ge, Y. Dai, and K. Li, Self-sustained Euler buckling of an optically responsive rod with different boundary constraints, Polymers **15**, 316 (2023).

[35] G. Graeber, K. Regulagadda, P. Hodel, C. Küttel, D. Landolf, T. Schutzius, and D. Poulikakos, Leidenfrost droplet trampolining, Nat Commun. **12**, 1727 (2021).

[36] Y. Kim, J. Berg, and A. J. Crosby, Autonomous snapping and jumping polymer gels, Nat. Mater. **20**, 1695 (2021).

[37] J. Liu, J. Zhao, H. Wu, Y. Dai, and K. Li, Self-oscillating curling of a liquid crystal elastomer beam under steady light, Polymers **15**, 344 (2023).

[38] K. Li, B. Zhang, Q. Cheng, Y. Dai, and Y. Yu, Light-fueled synchronization of two coupled liquid crystal elastomer self-oscillators, Polymers **15**, 2886 (2023).

[39] B. Liao, H. Zang, M. Chen, Y. Wang, X. Lang, N. Zhu, Z. Yang, and Y. Yi, Soft rod-climbing robot inspired by winding locomotion of snake, Soft Robot. **7**, 500 (2020).

[40] Y. Wang, J. Liu, and S. Yang, Multi-functional liquid crystal elastomer composites, Appl. Phys. Rev. **9**, 011301 (2022).

[41] K. M. Herbert, H. E. Fowler, J. M. McCracken, K. R. Schlafmann, J. A. Koch, and T. J. White, Synthesis and alignment of liquid crystalline elastomers, Nat. Rev. Mater. **7**, 23 (2022).

[42] S. Li, H. Bai, Z. Liu, X. Zhang, C. Huang, L. W. Wiesner, M. Silberstein, F. Robert, and R. F. Shepherd, Digital light processing of liquid crystal elastomers for self-sensing artificial muscles, Sci. Adv. **7**, eabg3677 (2021).

[43] M. Wang, Z. Cheng, B. Zuo, X. Chen, S. Huang, and H. Yang, Liquid crystal elastomer electric locomotives, ACS. Macro. Lett. **9**, 860 (2020).

[44] J. Zhang, Y. Guo, W. Hu, R. H. Soon, Z. S. Davidson, and M. Sitti, Liquid crystal elastomer based magnetic composite films for reconfigurable shape-morphing soft miniature machines, Adv. Mater. **33**, 2006191 (2021).

[45] K. Li and S. Cai, Modeling of light-driven bending vibration of a liquid crystal elastomer beam, J. Appl. Mech. **83**, 031009 (2016).

[46] R. Bai and K. Bhattacharya, Photomechanical coupling in photoactive nematic elastomers, J. Mech. Phys. Solids **144**, 104115 (2020).

[47] Y. Yu, L. Li, E. Liu, X. Han, J. Wang, Y. Xie, and C. Lu, Light-driven core-shell fiber actuator based on carbon nanotubes/liquid crystal elastomer for artificial muscle and phototropic locomotion, Carbon **187**, 97 (2022).

[48] N. W. Bartlett, M. T. Tolley, J. T. Overvelde, J. C. Weaver, B. Mosadegh, K. Bertoldi, G. M. Whitesides, and R. J. Wood, A 3D-printed, functionally graded soft robot powered by combustion, Science **349**, 161 (2015).

[49] M. Wehner, R. L. Truby, D. J. Fitzgerald, B. Mosadegh, G. M. Whitesides, J. A. Lewis, and R. J. Wood, An integrated design and fabrication strategy for entirely soft autonomous robots, Nature **536**, 451 (2016).

[50] Q. Cheng, X. Liang, and K. Li, Light-powered self-excited motion of a liquid crystal elastomer rotator, Nonlinear Dynam. **103**, 2437 (2021).

[51] Y. Chen, H. Zhao, J. Mao, P. Chirarattananon, E. F. Helbling, N. P. Hyun, and R. J. Wood, Controlled flight of a microrobot powered by soft artificial muscles, Nature (London) **575**, 324 (2019).

[52] D. Zhao, Y. Liu, and C. Liu, Transverse vibration of nematic elastomer Timoshenko beams, Phys. Rev. E **95**, 012703 (2017).

[53] D. Zhao and Y. Liu, Effects of director rotation relaxation on viscoelastic wave dispersion in nematic elastomer beams, Math. Mech. Solids **24**, 1103 (2019).

[54] L. Yang, L. Chang, Y. Hu, M. Huang, Q. Ji, P. Lu, and Y. Wu, An autonomous soft actuator with light-driven self-sustained wavelike oscillation for phototactic self-locomotion and power generation, Adv. Funct. Mater. **30**, 1908842 (2020).

[55] D. Ge, P. Xu, and K. Li, Self-sustained oscillation of a photothermal-responsive pendulum under steady illumination, Math. Probl. Eng. **2021**, 5531530 (2021).

[56] K. Korner, A. S. Kuenstler, R. C. Hayward, B. Audoly, and K. Bhattacharya, A nonlinear beam model of photomotile structures, Proc. Natl. Acad. Sci. USA **117**, 9762 (2020).

[57] A. S. Kuenstler, Y. Chen, P. Bui, H. Kim, A. DeSimone, L. Jin, and R. Hayward, Blueprinting photothermal shape-morphing of liquid crystal elastomers, Adv. Mater. **32**, 2000609 (2020).

[58] M. Parrany, Nonlinear light-induced vibration behavior of liquid crystal elastomer beam, Int. J. Mech. Sci. **136**, 179 (2018).

[59] D. Zhao and Y. Liu, Photomechanical vibration energy harvesting based on liquid crystal elastomer cantilever, Smart Mater. Struct. **28**, 075017 (2019).

[60] A. S. M. Rodriguez, M. Hosseini, and J. Paik, Hybrid control strategy for force and precise end effector positioning of a twisted string actuator, IEEE/ASME Trans. Mechatr. **26**, 2791 (2021).

[61] T. Würtz, C. May, B. Holz, C. Natale, G. Palli, and C. Melchiorri, The twisted string actuation system: Modeling and control, in *Proceedings of the 2010 IEEE/ASME International Conference on Advanced Intelligent Mechatronics* (IEEE, New York, 2010), pp. 1215–1220.

[62] T. Nagele, R. Hoche, W. Zinth, and J. Wachtveitl, Femtosecond photoisomerization of cis azobenzene, Chem. Phys. Lett. **272**, 489 (1997).

[63] L. B. Braun, T. Hessberger, E. Pütz, C. Müller, F. Giesselmann, C. A. Serra, and R. Zentel, Actuating thermo- and photo-responsive tubes from liquid crystalline elastomers, J. Mater. Chem. C **6**, 9093 (2018).

[64] H. Finkelmann, E. Nishikawa, G. G. Pereira, and M. Warner, A new opto-mechanical effect in solids, Phys. Rev. Lett. **87**, 015501 (2001).

[65] See Supplemental Material at http://link.aps.org/supplemental/10.1103/PhysRevE.108.054702 for videos associated with some of the figures.